Helium ion therapy compared to protons therapy using MCNP Monte-Carlo code

ABDESSAMAD DIDI*[1], HASSANE DEKHISSI[1], YJOU MOHAMED[1], RAJAA SEBIHI[2]
[1] Laboratoire de Physique Theorique, de Particules et Modelisation (LPTPM),
Department de Physique, Faculte des sciences, Universite Mohamed I, Oujda, Maroc
[2] Equipe ESMAR, Department de Physique, Faculte des sciences, Universite Mohamed V, Rabat

In this work, we are interested to study the hadron-therapy with charged particles, such as proton and helium, and we are investigated to simulate lateral and depth protons and helium dose, for delivering the most effective dose to the volume of the tumor, by protecting neighboring healthy tissues. The purpose of this article is to study and evaluate the potential benefits that the use of these particles could bring to the planning and implementation of medical treatment plans. To this end, the physical properties characterizing the helium and proton beams were analyzed using Monte Carlo simulation using MCNPX and MCNP6. In this study, however, one of the two codes gave results that did not agree with each other. This highlighted the need for a correct interpretation of the results obtained with Monte Carlo simulations, which must always be critically evaluated, especially in the absence of experimental comparison data, as in our case.

Keywords: hadron-therapy, MCNP6, MCNPX, depth dose distribution, lateral dose distribution.

I. INTRODUCTION

Hadron-therapy, also known as ion beam therapy, is a multidisciplinary field involving biology, medicine, physics, and engineering [1-2]. It is a specific type of oncology radiotherapy that uses fast hadrons, to achieve a better dose deposition, compared to conventional radiotherapy, which uses photons and electrons [3-4]. The development of hadron-therapy is part of the current evolution of radiotherapy, according to two important choices: The first choice is ballistics, which is visualized on the operational side during the optimization of the dose distribution in the tumor; take into account the adverse effects of healthy neighborhood tissue. The second choice is biological, which is visualized by an increase in the relative biological effectiveness of the radiation during a large linear energy transfer [3]. Currently, computational methods have been very extensively developed, either by the deterministic method or by the Monte Carlo method or by in vivo dosimetry [4].

II. MATERIALS AND METHODS

Some hadrons have been used for the treatment of solid tumors, such as neutrons, protons, and others [5-6]. However, in patients, three types of hadrons are used for the treatment of tumors: protons, helium and carbon ions [7-9]. The simulation codes are used to calculate the ion transport in the material, which was done using MCNP6 [10] and MCNPX [11].

In this study, we used the MCNP cross-section by application of ENDF/B-VII [12]. Two simulations took into account the same type of source, that is to say, a mono-energetic beam of helium ions, in the first place and then a proton beam in second place, the same geometry, and composition of the target are used in this work. They are many scientific studies [13-16] that have been done regarding the interactions between particles and matter using MCNP [17-20]. The target was modeled as a cylindrical water volume with the axis of symmetry in the direction of propagation of the incident beam, surrounded by air. The length of the target is 30 cm and a radius of 5 cm. The region of the air surrounding the water target with a length of 60 cm and a radius of 25 cm, in this simplified model (Fig.1) the total energy deposition was noted in cells of 0.01 cm wide in the direction of the incident beam. The simulations are carried out in a phantom, by two types of Monte-Carlo codes (MCNP6 and MCNPX). Figure 1 illustrates a simple geometry. In this study, two types of simulations are supported (lateral distribution and depth distribution) and two types of beam: the first using a proton beam of five different energies (50 MeV, 60 MeV, 80 MeV, 100 MeV and 150 MeV), the second helium beam of five different energies (50 MeV, 60 MeV, 80 MeV, 100 MeV, and 150 MeV). The absorbed dose, defined as the ratio of the average energy dE conferred by ionizing radiation in a volume element to the mass dm of matter in this volume, is expressed in units of gray (Gy), where 1 Gy = 1 J/kg [21].

$$Dose = \frac{dE}{dm}$$

Practically, the Bragg curve is the result of three interaction processes [22]: Shutdown, which causes the slowing of particles by the ionization process. Diffusion, which mainly affects the defection of the beam from the original direction. The nuclear interactions that cause the fragmentation of the target and then contribute to the broadening of the lateral beam and a tail of nuclear fragmentation after the peak. In addition, this effect also results in a reduction of beam fluency [23].

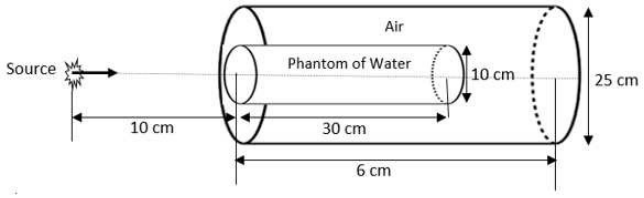

FIG. 1: Representative diagram of the geometric structure of the model

III. RESULTS

A. Helium ion beam

1. Depth distribution dose

The curves in Figure 2 represent a comparison between the depth of dose performance in a phantom created by a helium beam of different energies using the codes MCNP6 and MCNPX. All the patterns in Figure 2 are characterized by the "Bragg Peak": almost all of the irradiation dose is delivered in an extremely focused manner at a depth. Note in the case of a 50 MeV beam a remarkable coincidence in the dose distribution between the MCNP and the MCNPX the deposit depth of the entire dose was 5 cm (a). A coincidence between the results of the two codes is slightly modified at the peak level for 60 MeV (b) and 80 (c) (more intense dose value using the MCNPX) and with depths of 10 cm and 17 cm respectively. At 100 MeV (d) still, clear deference in Figure 2 between the depth dose found by the MCNP6 and that found by the MCNPX, the deposit of the entire dose was 25 cm deep. Recently, at 150 MeV the depth dose distribution varies clearly between 37 cm and 52 cm, and when the helium beam energy changes the deposit of the entire energy in-depth changes as well. The dose is more intense when the beam energy is low, and the depth is wider when the beam energy is greater. Note also that the variation of the results slightly varies when the calculation code is varied (f).

2. Lateral distribution dose

Figure 3 is a graphical representation of the lateral dose distribution in a phantom with a radius of 5 cm. The results show an acceptable proportion between MCNP6 and MCNPX, for a helium beam less than or equal to 80 MeV. By analyzing each curve in FIG. 3, the dose is equal to 33 MeV/g for a 50 MeV beam (a), for a 60 MeV beam a maximum dose value equal to 22.5 MeV/g (b)and for a beam with an energy of 80 MeV the dose is equal to 16 MeV/g (c). On the other hand, when the helium beam is equal to 100 MeV, the calculation results of the lateral dose distribution vary slightly between the types of Monte Carlo code used, MCNPX gives a value of 27 MeV/g and the code MCNPX gives the value of 24 MeV/g (d). When the helium beam is equal to 150 MeV (e), the maximum dose in the middle is equal to 10 MeV/g with the code MCNPX and 9 MeV/g for the code MCNP6. Figure 3 (f) shows a simulation series of all previously used beam energy. The dose is maximum when the beam intensity is low, but the dose is low when the beam intensity is maximum.

B. Proton beam

1. Depth distribution dose

Figure 4 shows the dose distribution at the penetration of a proton beam, five proton beams are involved energy 50 MeV, 60 MeV, 80 MeV, 100 MeV, and 150 MeV, their graphic presentation respectively are (a), (b), (c), (d) and (e), Figure (f) is the graphical presentation of all the depth distributions of the dose studied. We analyze the curves of Figure 4; we find that the energy deposition is faster for the energy of 50 MeV; the Bragg Peak is at the depth

of 2 cm with a dose of 1 MeV/g (a).

2. *Lateral distribution dose*

Figure 5 shows the lateral dose distribution for different energies. The results show a proportion between the two simulation codes. The calculation of the lateral distribution of the dose at 50 MeV is maximum in the middle is equal to 8.5 MeV/g, the dose is canceled after 2 cm in diameter (a). The calculation of the lateral dose at 60 MeV is coincidental between the two codes (MCNP6 and MCNPX) is maximum in the middle is equal to 6 MeV/g (b). From Figures 3 and 4, which represent lateral distribution and depth dose in a phantom, under the effect of a proton beam of varied energy (50 MeV, 60 MeV, 80 MeV, 100 MeV, and 150 MeV), we can say that the proton and helium beam holds an important place in the medical field and especially in radiotherapy.

Figure 6 represents a comparison between the depths of dose deposition by two beams in a tumor located at 5 cm of depth. In black the dose produced by the beam at 50 MeV of helium and the red the dose produced by a beam of 80 MeV produced by the proton, beam energy are deferent but the depth and the same, so with two different energies can destroy a tumor. The estimation of errors related to the simulation between 1% and 3% because of the calculation tools, the Monte Carlo calculation gives results closer to reality when using a larger historical number.

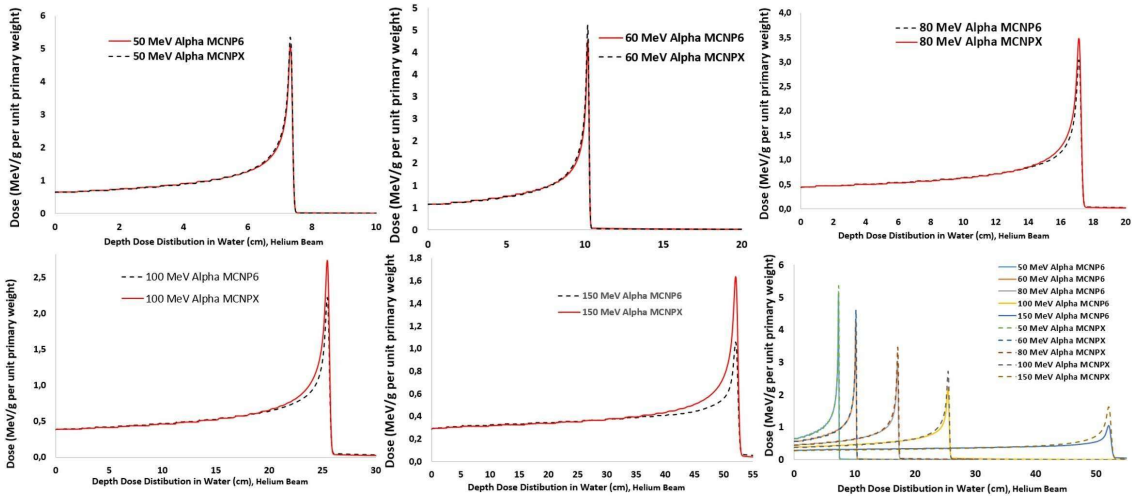

FIG. 2: Depth-dose distribution of different helium Beam Energy in water calculated using MCNP6 and MCNPX

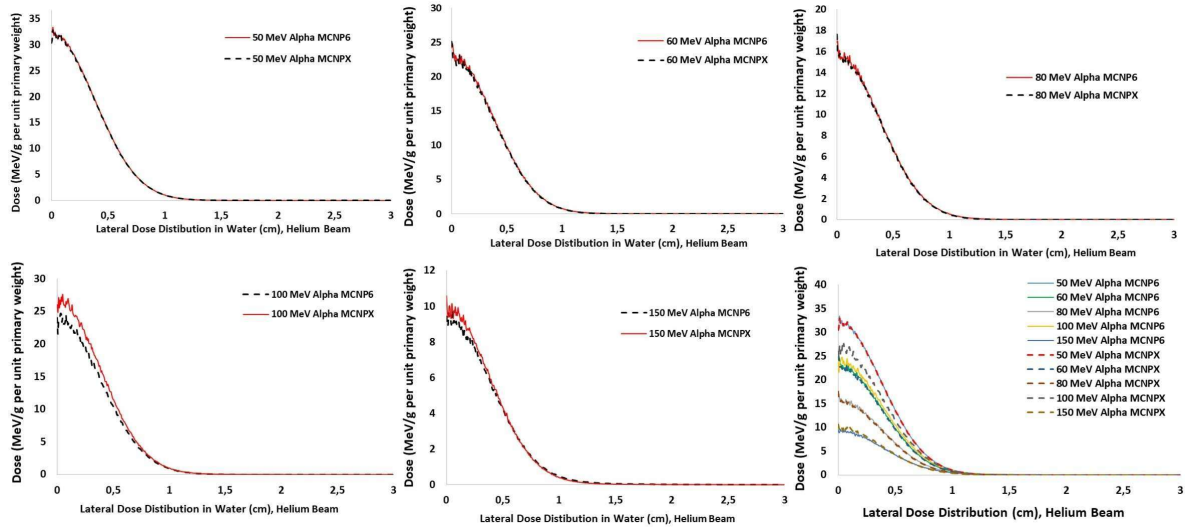

FIG. 3: Lateral dose distribution of different helium beam energy in water calculated using MCNP6 and MCNPX

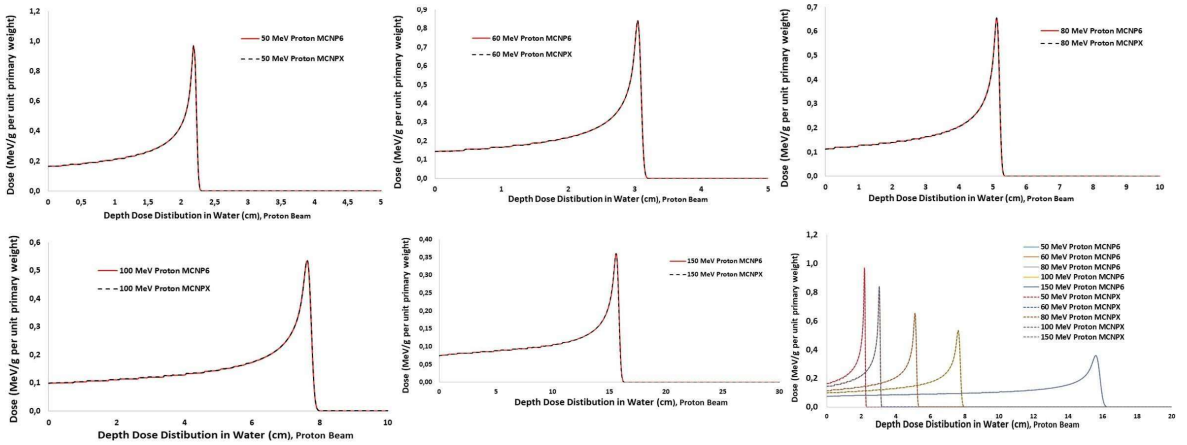

FIG. 4: Depth-dose distribution of different proton beam energy in water calculated using MCNP6 and MCNPX

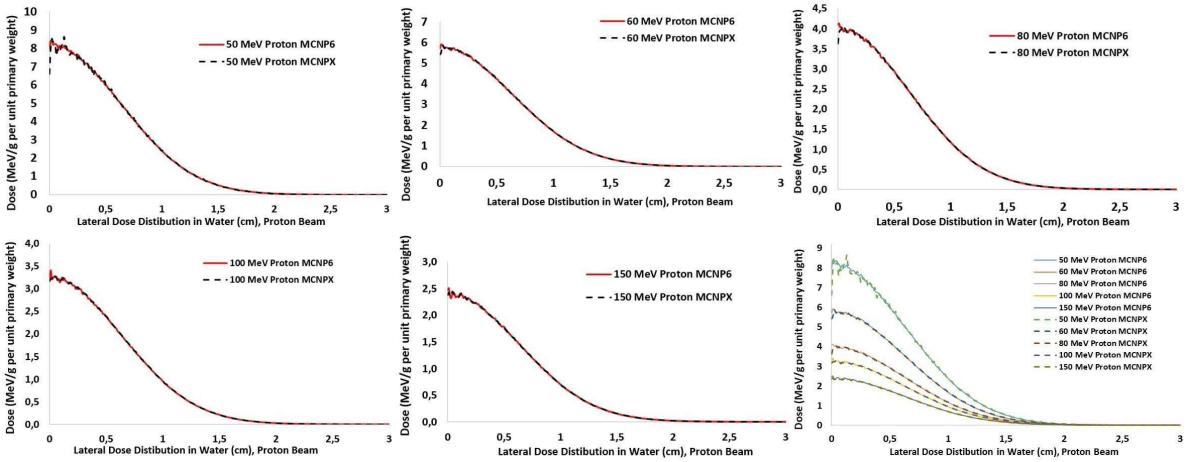

FIG. 5: Lateral dose distribution of different proton beam energy in water calculated using MCNP6 and MCNPX

IV. DISCUSSION

A cyclotron or a synchrotron produces helium, like protons [24]. For a helium-4 ion with an atomic number Z= 2 and a mass number A = 4, which means that, with respect to a proton, any electric field is multiplied by 2 but the inertia is multiplied by 4. The behavior of light ions in the matter is quite similar to protons, with structural variations, in these variations that are the possible arguments that could support a separate development of ion therapy. In addition, the Bragg peak is much more pronounced in the case of helium ions (He), which means that at the same dose the peak, we obtain less energy deposition in the tissues that preceded the peak is also thinner, which a priori allows a better precision. When particles travel in and interact with a medium, they have the ability to transfer or deposit energy in the medium, as the case may be. When measuring energy deposition at different depths (PDD), it is observed that electrons and protons deposit most of the energy at close range [25]. However, the protons and alpha ions deposit their dose during the last interactions, as shown in Figures 2 and 4. This particular characteristic of the protons and helium ions, known as Bragg Peak, allowed to initiate its use for the control of tumors because of the possibility of depositing with great precision the energy and to attenuate the effects on the healthy tissues.

The interactions of protons in matter can interact in three different ways: first, they slow down under the effect of their collisions with the middle electrons, second, they are divided by collisions with the nuclear nucleus or third they can directly interact with the nucleus and causing the generation of secondary particles; this process called nuclear braking and dispersion. Braking and dispersion are by electromagnetic interactions between the charge of the proton and the electrons of the nucleus. The dose depth curves evidenced by proton and helium beams (Figure 2 and Figure 4) are completely different from the photon and neutron beams because the charged particles give the maximum dose close to the end of their path in tissue and give birth to Bragg's spike. It is always remarkable that the existence of the Bragg peak is a direct consequence of the fact that for all the light ions of the dependence of the energy loss is well follows a simple mathematical law which depends on the energy losses drawn in the function of the residual course R, are approximately given by law:

$$R^{0.45}$$

Protons are beneficial in Intensity Modulated Radiation Therapy (IMRT) for three physical aspects:

a- They deposit their maximum energy density in the Bragg Peak at the end of their course, where they can produce severe cell damage while protecting healthy tissue that is traversed and deeper than the tumor.

b- They enter the patient virtually without diffusion.

c- Being charged, they can easily be formed in focused beams and scanned with penetration of varying depth, so that all parts of the tumor is precisely and quickly irradiated.

Thus, a beam of protons or light ions, allows a highly consistent treatment of deep tumors, with precision to the millimeter, ensuring a minimal dose to the surrounding tissues. In addition, a proton beam as a light particle, allows highly consistent treatment of deep tumors, with precision.

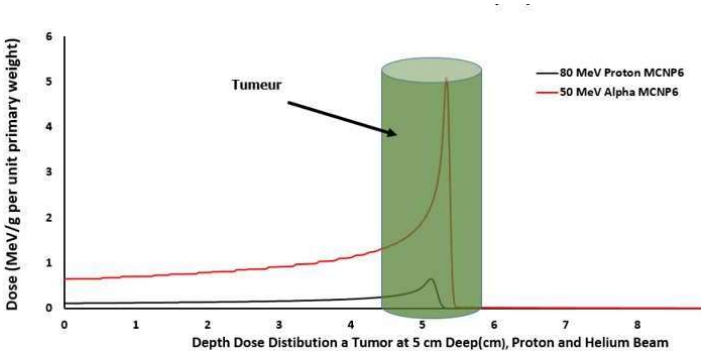

FIG. 6: Depth-dose distribution of 80 MeV proton beam and 50 MeV helium beam in water calculated using MCNP6

v. CONCLUSION

It can be said that the use of proton beams or a helium ion beam of varied energy allows the consistent treatment of localized tumors close to the skin or deep tumors according to the energies and the projectile used. The treatment using light ions as our study consists of sending particles into the tumor in order to destroy them by taking into account the risk tissues. Because of their weight and their energy charge relative to the proton. One of the few centers in the world to offer ion radiotherapy. In this study, we discussed two types of simulation; first using the MCNPX and the second using the MCNP6, the results produced by the two codes are in total comfort with real and experimental results [26]. The validation of our results with experimental studies shows compatibility if uses MCNPX in the case of basic energy also in the case of high energy the MCNP6 shows a significant compatibility [27].

References

[1] W. Kilby et-al., Technology in cancer research **9**, 433-452 (2010).

[2] D. Schardit, Theory, Experiments and Applications 55- 86 (2016).

[3] L. Feuvret et-al., Cancer Radiothérapie **19**, 519-525 (2015).

[4] CM. Charlie Ma et-al., Proton and carbon ion therapy. Boca Raton, FL: CRC Press Pub. **1**, 209-220 (2013).

[5] A. Kosuneh et-al., Radiotherapy and Oncology **29**, 327- 335 (1993).

[6] F. Binder et-al., Estimation nationale de l'incidence et de la mortalité par cancer en France entre 1980 et 2012. partie 1, Tumeurs solides. Saint-Maurice (Fra): Institute de veille sanitaire,

[7] C. -A. Tobias et-al., The American journal of roentgenology, radium therapy, and nuclear medicine **67**, (1952).

[8] M. Suzuki et-al., International Journal of Radiation Oncology Biology Physics **48**, 241-250 (2000).

[9] Serena Marta Valle, UNIVERSITRA DEGLI STUDI DI PAVIA Facolta di Scienze Matematiche Fisiche e Naturali, HELIUM ION BEAMS FOR EYE TREATMENT: AN IN SILICO

INVESTIGATIONS, (2014).

[10] A. MCNP6, MCNP (2014) X-6 Monte Carlo Team, N-Particle Transport Code System Including MCNP6.1, and Data Libraries, MCNP6 User's Manual, Code Version 6.1.1beta, LA-CP-14-00745.

[11] D. B. PELOWITZ, MCNPX, MCNPX: MCNPX User's Manual Version 2.7.0, LA-CP-11-00438, Los Alamos National Laboratory

[12] S.G. ENDF., Evaluated Nuclear Reaction Data File (ENDF), Available online at: http://www.nndc.bnl.gov/exfor.htm Los Alamos, (2017).

[13] A. Didi et-al., International Journal of Nuclear Energy Science and Technology **12**, 313-323 (2018).

[14] A. Didi et-al., International Journal of Nuclear Energy Science and Technology **12**, 324-327 (2018).

[15] A. Didi et-al., Moscow University Physics Bulletin, **73**, 618-621 (2018).

[16] A. Didi et-al., Moscow University Physics Bulletin **73**, 612-617 (2018).

[17] A. Didi et-al., Moscow University Physics Bulletin **72**, 460-464 (2018).

[18] A. Didi et-al., Moscow University Physics Bulletin, **74**, 364–368 (2019).

[19] A. Didi et-al., Moscow University Physics Bulletin **72**, 465-469 (2017).

[20] A. Didi et-al., Nuclear Engineering and Technology **49**, 787-791 (2017).

[21] F. Michael et-al., Radiation Physics and Radionuclide Decay, in Handbook of Radioactivity Analysis (Third Edition) (2012).

[22] W. H. Bragg et-al., Philosophical Magazine 726-738 (1904).

[23] D. S. Bollinger et-al, AIP Conference Proceedings 1655, 070002 1-7 (2015).

[24] H. OWEN et-al, Int. J. Mod. Phys. A 1-54 (2013).

[25] R. Acciarri et-al, First Observation of Low Energy Electron Neutrinos in a Liquid Argon Time Projection Cham- ber 1-20 (2017).

[26] D. Schulz-Ertner et-al, Int. J. Radiat. Oncol. Biol. Phys. **58**, 631-40 (2004).

[27] M. Kawashima et-al, J. Clin. Oncol. **23**, 1839-46 (2005).